DIMACS Series in Discrete Mathematics
and Theoretical Computer Science

Modeling the Invasion and Spread of Contagious Diseases in Heterogeneous Populations

Wayne M. Getz, James O. Lloyd-Smith, Paul C. Cross, *Shirli Bar-David, Philip L. Johnson, Travis C. Porco, and María S. Sánchez

Abstract. The evolution of disease requires a firm understanding of heterogeneity among pathogen strains and hosts with regard to the processes of transmission, movement, recovery, and pathobiology. In this chapter, we build on the basic methodologies outlined in the previous chapter to address the question of how to model the invasion and spread of diseases in heterogeneous environments, without making an explicit link to natural selection—the topic of other chapters in this volume. After a general introdution in Section 1, the material is organized into three sections (Sections 2–4). Section 2 covers heterogeneous populations structured into homogeneous subgroups, with application to modeling TB and HIV epidemics. Section 3 reviews a new approach to analyzing epidemics in well-mixed populations in which individual-level variation in infectiousness is represented by a distributed reproductive number [**51**]—in particular, the expected number of secondary cases due to each individual is drawn from a gamma distribution, yielding a negative binomial offspring distribution after stochasticity in transmission is taken into account. In Section 3, we discuss ideas relating to superspreading events, as well as the best way to characterize the heterogeneity associated with transmission in real epidemics, including SARS, measles, and various pox viruses. Section 4 deals with individual-based approaches to modeling the spread of disease in finite populations with group structure, focusing on several issues including interactions among movement, transmission, and demographic time-scales, the effects of network connectivity on the spread of disease, and the spread of disease in invading or colonizing hosts. The applications in Section 5 focus on bovine TB (BTB) in an African buffalo population and the potential for BTB to invade a colonizing Persian fallow deer populations.

1. Introduction

In the previous chapter [**35**], a set of methods for modeling epidemics in homogeneous populations was presented. In this chapter, we use these methods to address theoretical and applied problems on the invasion and spread of contagious diseases in heterogeneous populations.

Population heterogeneity can often be represented by dividing a host population into homogeneous subgroups based on spatial location, sex, behavior, genetics or

*Authorship is alphabetical from here onwards.

other factors. Analysis of basic epidemic properties in such multi-group or multi-type populations is well-developed [**2, 5, 25, 26**], but more advanced questions and applications continue to motivate research in this important area.

Heterogeneous populations with homogeneous subgroups can broadly be divided into those with and those without inter-group transitions on time scales relevant to the analysis. Another important distinction is whether transmission occurs among individuals in different groups or only among individuals within the same groups. These two criteria define a basic taxonomy of multi-group disease models, for which we provide several examples below. For instance, a population may be structured into groups according to some unchanging social categorization (hence no transitions among groups) or all individuals are potentially able to interact with another (hence transmission among groups is possible) but interaction rates are much greater within than among groups.

In this chapter, we present three approaches to dealing with heterogeneity, using several of our own recent studies as illustrative examples. The first approach is the relatively simple approach of dividing a heterogeneous population into a finite number of homogeneous subpopulations and then modeling the dynamics of the epidemic using a system of discrete difference equations with application to tuberculosis and HIV/AIDS in humans. The second approach is an application of stochastic branching process theory where the *individual reproductive number* associated with each infectious case (i.e. the expected number of new infections caused by each infected individual) is itself a random variable rather than a constant. We apply this approach to analyzing outbreak data from several important diseases including SARS, measles, smallpox, pneumonic plague, and other viral diseases.

The third approach is the use of individual-based discrete time stochastic simulation models, and their application to investigating how the timescales of host mixing and recovery from disease interact to determine the probability of a pandemic. We also discuss their use in modeling the spread of disease in a network of individuals characterized by an empirically derived association matrix for the purposes of obtaining insight into the spread of bovine tuberculosis in the African buffalo (*Syncerus caffer*) in the Kruger National Park, South Africa.

In this chapter, for convenience of presentation, we refer to the 25 equations presented in the previous chapter [**35**] using the numbers they have been designated in that chapter, such as [**35**, Equation number].

2. Interconnected homogeneous subgroups: TB and HIV

Classification of populations into groups is almost always problematic because group boundaries are ad-hoc. In modeling the spread of HIV, for example, it would be useful to be able to organize individuals into groups based on sexual preference, practice, and level of promiscuity. In many ways, an individual's behavior is better described by continuous rather than categorical variables. Nevertheless, categorical approaches are most often taken [**63**] because of their relative simplicity compared to approaches using a continuous descriptive variable. For example, the Actuarial Society of South Africa's (ASSA) official model for projecting the HIV/AIDS epidemic in South Africa divides the population into four risk groups based on categorization of sexual behavior, without allowing movement among groups. In reality, some individuals are bound to change their behavior as they learn more

about the epidemic, as they age through time, or as their disease symptoms progress (e.g. [**37, 42, 43**]).

A critical source of heterogeneity in a population challenged with HIV is the presence of other diseases that can act as cofactors, particularly venereal diseases that enhance opportunities for the spread of HIV. Conversely, because it impairs immune function, HIV infection can have dramatic impacts on host response to other diseases, particularly the so-called opportunistic infections [**44**], one of the most important of which is tuberculosis (TB) [**41**]. For many TB-infected individuals the infection remains latent and has little effect on their health, but infections become acute and deadly once individuals are immunocompromised. From a TB epidemic point of view, the course of the disease is going to be vastly different in individuals infected with HIV than in otherwise healthy individuals [**1, 20, 52, 68**]. Accordingly, when considering the interaction of these two epidemics, we can formulate a full TB-HIV model in a homogeneous population, where we include the transmission and progression dynamics of both diseases. The caveat for this framework is its high level of complexity, which is compounded by the fact that there is a great level of uncertainty in the parameter values characterizing the epidemiological features of both TB and HIV.

Alternatively, we can begin by modeling TB in a population in which a certain proportion of individuals have HIV, without explicitly modeling the HIV epidemic itself [**65**]. This approach is justified by the fact that the impact of TB on the epidemiology of HIV appears to be less dramatic than that of HIV on TB [**4, 21, 24, 53**]. Under these assumptions, the background HIV structure is not static because we allow individuals in different HIV groups to progress according to the WHO disease staging system (susceptible, clinical stages I to IV, and dead). The essential simplification is that we model the transition of susceptibles to HIV stage I using a recruitment process, based on historical patterns obtained from empirical data, rather than modeling HIV transmission in detail. Essentially, we have a TB only epidemic model, embedded within a population that is heterogeneous with respect to HIV stages [**22, 29, 57, 61**]. This kind of framework may prove to be just as informative as a full TB-HIV model if we are trying to understand the course of the TB epidemic within a relatively short period of time (e.g. 10–20 years), because input of the best estimates of HIV incidences from current data are likely to be as reliable as predictions from an HIV transmission model over the period of concern.

Here we sketch out how we are using an incidence input approach to develop a model of a TB epidemic occurring in a population that is heterogeneous with respect to HIV status. The model is constructed as outlined in Section 6 of the previous chapter [**35**], but it has many more disease classes because the aetiology and clinical presentations of TB are very complex (Figure 1A). Because one of our motivations for developing a TB-HIV model is to determine the potential impact of reducing treatment duration in TB infected patients in areas of high HIV prevalence, the model outlined below has a strong focus on TB treatment classes progressing over a monthly time scale. This level of time resolution entails 42 different categories of disease/treatment classes for the TB epidemic alone.

Specifically, individuals newly infected with TB can progress to active disease at a slow or fast rate, and those with an active infection can be classified as sputum-smear positive or negative. Among those individuals with an active infection, a

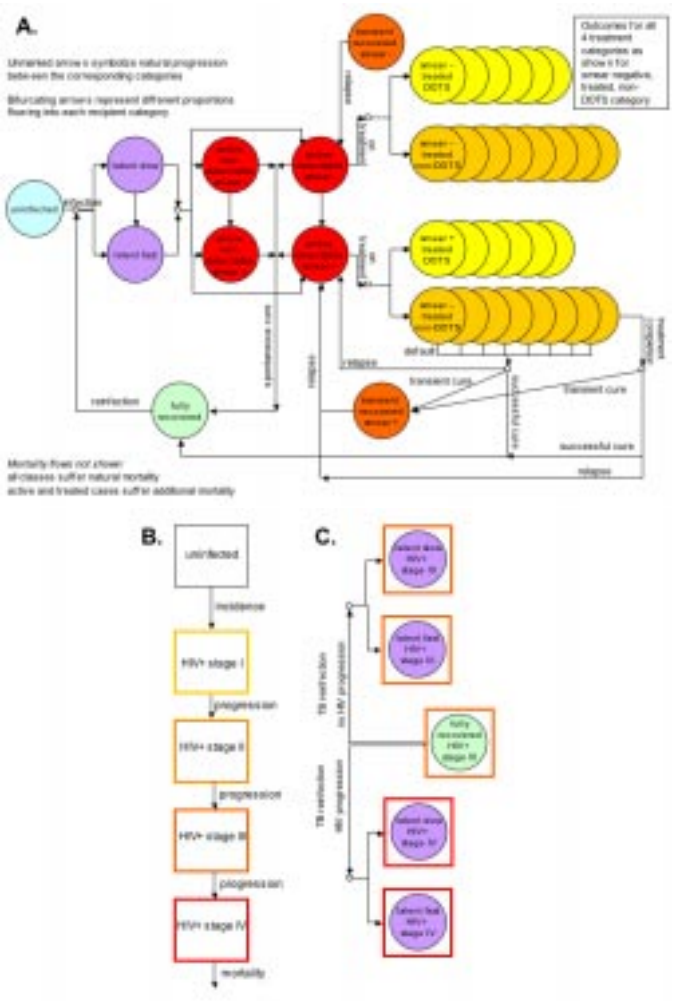

FIGURE 1. TB in a homogenous (**A.**) and an HIV impacted population (**B.** and **C.**). Categories and flows included in the TB/HIV model used to determine the impact of reduced TB treatment duration on the TB epidemic in areas of high HIV prevalence. **A.**) TB transmission, progression, treatment, and mortality is represented by a total of 42 categories. **B.**) HIV incidence, progression, and mortality is accounted for by 5 stages (HIV- and HIV+ stages I-IV). C.) TB reinfection flow exiting the "fully recovered HIV+ stage III" category, and entering the slow and fast latent TB categories in HIV+ stage III for HIV non- progressors, and HIV+ stage IV for HIV progressors. Each HIV stage includes the 42 TB categories for a total of 210 combined TB/HIV categories. For simplicity we have chosen to represent the TB categories and HIV stages separately in **A.**) and **B.**), while in **C.**) we show one representative TB process occurring within the context of HIV progression. In effect, the pattern displayed in **C.**) is used for all TB categories, with HIV- individuals becoming infected at a fixed incidence level, HIV+ individuals in stages I-III progressing to the next stage at a fixed rate, and HIV+ individuals in stage IV dying from AIDS also at a fixed rate.

certain fraction can be detected and placed on treatment, others are undetectable (due to subclinical symptoms or lack of access to health care) and will never become treated, while some can recover completely without ever being treated. At each time step individuals within the detectable category are placed on treatment at a given rate, and can then enter either a DOTS or a non-DOTS regimen (DOTS stands for Directly Observed Treatment Short-course, but represents many more aspects of a well-run governmental TB control program—see [**23**]). We model the impact of treatment regimens that take different lengths of time to cure TB. Treated individuals can recover transiently or completely, or relapse to active disease. Flows among these categories were chosen to reflect the most critical processes determining TB incidence, prevalence, and mortality under different treatment regimens, paying particular attention to case detection, default, relapse, and reinfection.

In the combined TB-HIV model, we assume HIV-negative individuals become infected with HIV at a fixed input level given by reported incidence levels, and flow into the corresponding TB category of individuals that are in stage I of their HIV infection. HIV-positive individuals then progress through the four HIV stages, for a total of 42×5 different TB/HIV categories (Figure 1B). Individuals in HIV stage IV die of AIDS according to a fixed HIV mortality rate. We allow for HIV to affect TB infection, progression, and mortality rates—and vice-versa. All TB processes, together with the background mortality and HIV mortality, are modeled as competing rates within a continuous and deterministic framework that is updated on a discrete monthly time step. This is an approximation to the exact solution of a deterministic model [**35**, Equation (6.4)], which allows all processes to occur simultaneously but restricts each individual to undergo one state transition per time step (unless the model is specifically adjusted to allow multiple transitions). HIV progression from stages I through IV occurs simultaneously with progression through various TB stages. At each time step, any given individual can progress in both diseases, in only one, or in neither.

Preliminary results indicate that a 2- compared with a 6-month treatment regime may offer important benefits that appear to reduce when HIV prevalence is high. The model is being used to investigate this reduction in benefits in more detail under new drug scenarios that include increased treatment compliance by patients [**9, 72**], reduced relapse after treatment completion [**30**], and enhanced case detection [**10, 31**].

3. Migrants and the spread of disease

In Section 8 of the previous chapter and Section 2 of this chapter, we presented models in which individuals respectively 1.) do not make transitions among non-disease categories of individuals and 2.) make transitions along a unidirectional chain of categories. Here we generalize these approaches by, in theory, permitting any individual in any category to move to any other category, where movement in the absence of disease is defined by a *migration matrix* $M(k)$ with elements $M_{ij}(k)$ representing the probability that an individual in category i moves to category j during time interval $[k, k+1]$, $i, j = 1, \ldots, n$ [**64**]. This approach generalizes the above mention earlier sections, and it is applicable to modeling epidemics over a region consisting of several urban areas or in animal populations that have an identifiable group (e.g. troop, pod, colony, herd) or metapopulation structure [**34, 36, 38, 40, 80**].

We begin by considering a population structured into n_g identifiable groups. For generality, we also divide the population by gender and include age structure, because movement rules among animal groups are very often influenced by gender and age of individuals. This level of generality, however, can turn into a notational nightmare. Thus one of our goals in this section is to present a notation that does not obscure the structure of the equations themselves. There are many ways to do this—our goal is to preserve the macrostructure in the equations while choosing representations that are mnemonic where possible.

The notation is built around the symbol Z, where $Z = X$ denotes females and $Z = Y$ males (the obvious mnemonic being the genetic context of X and Y chromosomes). A superscript $U = S, E, I, R(D, V)$ is used to denote disease class (where E, I, V etc. may be staged: e.g., I_l, $l = 1, \ldots, n_l$). Also, a subscript $a = 1, \ldots, n_a$ is used to denote age and a subscript $i = 1, \ldots, n_g$ is used to denote group (e.g. herd etc.). Thus the variable represents the number or density of individuals of gender Z, disease class U, age a, and group i. As in the previous section, we avoid the additional level of subscripting, by using $\pi = \alpha, \gamma, \mu$ etc., rather than p_π to represent transition probabilities (or proportions in large populations represented by deterministic models). We also use the same convention to refer to the migration parameters, but with an additional superscript needed to denote gender and another subscript needed to denote the proportion of individuals leaving group i that move to group j—that is, the migration parameters have the form $M^{ZU}_{aij}(k)$, which can be viewed as an $n_g \times n_g$ migration matrix for each gender, age and disease class of host. With this notation, using EPI to denote terms controlling disease class transitions and DEMOG to denote terms controlling demographic transitions (aging, births, deaths) all equations have the generic form

$$\begin{aligned} Z^U_{a+1\ i}(k+1) &= \mathrm{EPI}^{ZU}_{ai}(k) + \mathrm{DEMOG}^{ZU}_{ai}(k) \\ &\quad + \sum_{i=1,\ i\neq j}^{n_g} \left(M^{ZU}_{aji}(k) Z^U_{aj}(k) - M^{ZU}_{aij}(k) Z^U_{ai}(k) \right). \end{aligned} \tag{3.1}$$

We will not elaborate further on the structure of the terms in EPI and DEMOG in this section. We already have a sense from our models in Section 2 what form the EPI terms might take, while DEMOG terms follow the type of structure found in Leslie matrix formulations of age-structured models (e.g. see [**17**] for an example in the context of vaccinating African buffalo to control bovine TB). In terms of the movement process, we generally expect the coefficients $M^{ZU}_{ij}(k)$ to depend on the state of each group in our population (e.g. [**80**]), and to reflect a spatial topology typically represented by a set of parameters ξ_{ij} characterizing the "distance" (Euclidean or otherwise) between groups i and j over the time interval $[k, k+1)$. Dependence on group size might be quite complex, as discussed more fully in [**50**].

The primary issue we want to focus on in this section is the fact that in group structured systems of the type modeled by equation (3.1), we can define a matrix $\mathbf{R}_0$ of elements R_0^{ij} defined to be the expected number of individuals in group j that will be infected directly (i.e. in the next generation) by an individual infected in group i. We will return to the question of how to calculate $\mathbf{R}_0$, but once calculated it can be used to derive the expected number infected in the offspring generation for different situations. For example, if an infective is introduced to group j at time $k = 0$, then, in an otherwise susceptible population, the expected number infected

in the offspring generation is

$$R_0^{\bullet j} := \begin{pmatrix} R_0^{11} & \cdots & R_0^{1j} & \cdots & R_0^{1n} \\ \vdots & \vdots & \vdots & \vdots & \vdots \\ R_0^{n1} & \cdots & R_0^{nj} & \cdots & R_0^{nn} \end{pmatrix} \begin{pmatrix} 0 \\ \vdots \\ 1 \\ \vdots \\ 0 \end{pmatrix} = \sum_{i=1}^{n} R_0^{ij}.$$

Similarly, if an infective is introduced into group j with probability w_j at time $k = 0$ (this probability could be proportional to the initial group size or determined by its location on a landscape) then, in an otherwise susceptible population, the expected number infected in the offspring generation is

$$R_0^w := \sum_{i=1}^{n} \sum_{j=1}^{n} w_j R_0^{ij}.$$

Diekmann and Heesterbeek [**26**] have developed methods for generating the matrix $\mathbf{R}_0$, which they have dubbed the *next-generation matrix*. This matrix can also be generated numerically through simulation; but no example of this for a relatively detailed system has been published to date. If the next-generation matrix is irreducible and acyclic, its dominant eigenvalue is the basic reproduction number intrinsic to the system (as opposed to that defined above for the vector $\mathbf{w}$ of introduction probabilities) [**26**]. A more detailed discussion of the properties of the next-generation matrix can be found in Ovoskainen and Grenfell (2003).

An SIR model of the form (3.1), in a system without age or gender structure, has been analyzed by Hagenaars et al. [**38**] to consider how disease persistence is influenced by the tradeoff between the number of groups n_g and the initial group size $N_i = \hat{N}$, $i = 1, \ldots, n_g$, when the total initial population size $N_{\text{Tot}} = n_g \hat{N}$ is fixed. This model assumes that individuals in one group contact individuals in any other group at a relative rate ε, which implies that $f(\varepsilon) = \frac{1}{1+\varepsilon(n_g-1)}$ is the fraction of contacts with individuals from one's own group, with the rest equally distributed among the other groups. They also assume a relatively simple demographic component in which 1.) the birth and immigration rates are balanced by death and emigration rates, 2.) the migration is to a population that is external to the structured group of interest, and 3.) the external population is at constant disease prevalence. Their stochastic analysis of this model reveals that: "... if the overall transmission potential is kept fixed, increasing the level of spatial heterogeneity typically results in a decrease in disease persistence. For weak spatial coupling between subpopulations, the persistence changes as a function of coupling can be understood in terms of rescue effects. For intermediate and strong spatial couplings, coherence effects become important." Here, rescue effects imply that fade out of disease in one group is followed by reinfection from another group [**14**]. Also coherence in the context of relatively slow diseases implies similar levels of incidence in all groups, which for fast diseases can take the form of synchronized oscillations.

4. Individual heterogeneity in well-mixed populations

4.1. The individual reproductive number. For the past 25 years analysis of epidemic dynamics has centred on the basic reproductive number, R_0, which

is the expected number of new infections due to each infectious individual in a wholly susceptible population [**39**]. Models of homogeneous populations usually use a point estimate of R_0, implicitly assuming that every individual has the same degree of infectiousness. In reality, however, the infectiousness of each individual (as manifested by the number of secondary cases they cause) varies due to a complex blend of host, pathogen and environmental factors. The joint action of these factors leads to continuous variation in infectiousness and distinct risk groups often cannot be recognized *a priori*, thereby hampering our ability as modelers to represent this heterogeneity using group structure as described in the previous section.

To account for this variation, we introduce the individual reproductive number, ν, defined as the expected number of new infections that a given individual in the current generation will cause in the next generation [**51**]. At the population level, ν has some probability distribution that can be fitted to datasets describing the observed distribution of secondary cases caused by each individual (i.e. the empirical realization of the offspring distribution introduced in Section 7 in the previous chapter). The actual number of cases caused by each individual will vary stochastically around ν, so the realized offspring distribution will be a compound distribution with the form Poisson(ν) (i.e., a Poisson with parameter ν that is itself distributed). In a completely homogeneous population, where all individuals have identical infectiousness $\nu = R_0$, the offspring distribution will be Poisson as discussed in Section 7 of the previous chapter [**35**]. If all individuals transmit at the same rate (i.e. they have equal transmission coefficients β) and exponentially-distributed infectious periods (i.e. they have constant per capita rates of recovery or death), then ν is distributed exponentially with mean R_0 and the offspring distribution is geometric [**70**]. These two scenarios represent the standard assumptions used in homogeneous population models.

To allow for a more flexible degree of individual variation in infectiousness, we propose a model with a gamma-distributed ν. Gamma distributions are a useful two- parameter family of distributions for developing epidemic theory in heterogeneous populations, because they are unimodal and non-zero only on $(0, \infty)$. More important for the development of branching process theory, however, the offspring distribution arising from a population with gamma-distributed individual reproductive number ν is a negative binomial distribution. Further, this model is a generalization of the two conventional models (Poisson and geometric offspring distributions), as described below. The negative binomial distribution is typically expressed in terms of a scale parameter p and a dispersion parameter k. To emphasize the link with epidemiological models, we deviate from this practice and use the notation $\phi^{\mathrm{NB}}_{R_0,k}$ to denote a negative binomial offspring distribution with mean R_0 related to p and k by the equation

$$R_0 = k\left(\frac{1}{p} - 1\right). \tag{4.1}$$

The probability generating function for negative binomial distribution has the form

$$\underline{\text{Negative Binomial}}\ \ \phi^{\mathrm{NB}}_{R_0,k}:\ g(z) = \left(1 + \frac{R_0}{k}(1-z)\right)^{-k}.$$

As mentioned in Section 7 of the previous chapter, the probability q_0 that an infectious individual in the parent generation will not transmit to anyone in the

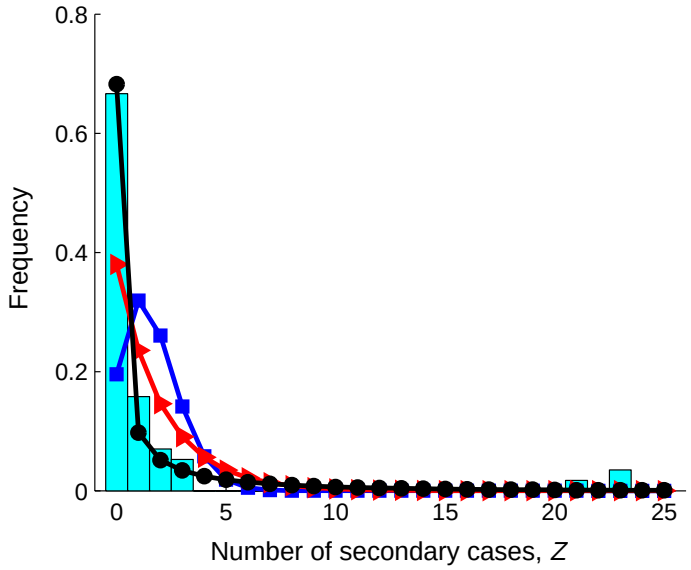

FIGURE 2. Empirical offspring distribution from the 2003 SARS outbreak in Singapore [**48**]. Bars show observed frequency of Z, the number of individuals infected by each case; lines show maximum likelihood fits for $Z \sim$ Poisson (squares), $Z \sim$ geometric (triangles), and $Z \sim$ negative binomial (circles).

offspring generation is $g(0)$, from which it follows for the negative binomial that

$$q_0 = \left(1 + \frac{R_0}{k}\right)^{-k}. \tag{4.2}$$

The Poisson and geometric distributions are special cases of the negative binomial distribution with $k \to \infty$ and $k = 1$, respectively.

During a number of recent epidemics, contact tracing of cases provided sufficient data for the construction of empirical offspring distributions to which Poisson, geometric and binomial distributions could be fitted. An example of this data for the SARS outbreak in Singapore, 2003 [**48**], is illustrated in Figure 2. Maximum likelihood methods can be used to find parameters of the negative binomial, Poisson, and geometric distributions that best fit these data. Of course, because of its extra parameter, the negative binomial distribution will always provide a better fit but the Akaike information criterion can be used to assess whether the improvement in fit over the one-parameter Poisson or geometric models is sufficient to merit inclusion of the extra parameter (e.g. see [**13**]). Further, bootstrap methods [**32**] can be used to estimate confidence intervals for the parameters characterizing these best-fitting offspring distributions. The results of such an exercise for 14 different disease datasets are summarized in Table 1, where we use $\hat{}$ to denote estimated values of the parameters R_0 and k. The Akaike weights reported in Table 1 represent the probability that each model is the best choice to represent the data of the three candidate models considered. The datasets include well-traced single outbreaks, combinations of data from multiple outbreaks, and surveillance data tracking the

first generation of many introductions of a disease. Note that many of the datasets, particularly measles and smallpox, pertain to populations with high levels of vaccination, so observed heterogeneity may reflect differences among vaccinated and unvaccinated individuals rather than intrinsic host or pathogen characteristics. More details pertaining to data, methods and results are given in Lloyd-Smith et al. [**51**].

A large degree of individual variation in infectiousness is evident in almost all of the 14 datasets analyzed in Table 1. For five of the disease datasets, the 90% confidence intervals for the negative binomial dispersion parameter k are bounded below 1, indicating that only the negative binomial offspring distribution can represent the observed patterns. The best estimate of k for 11 of the datasets suggests that heterogeneity is either greater or much greater than that arising from an exponential distribution of infectiousness (i.e. best-fit $k < 1$). Only one dataset exhibited sufficient homogeneity in infectiousness that the Poisson model was favored by the Akaike weight model-selection technique. This was Ebola hemorrhagic fever with the most likely value for k estimated to be $\hat{k} = 5.1$; this dataset had only 13 index cases and contact tracing was probably incomplete, so our confidence in this result is limited.

In half of the epidemics the best estimate for k was $\hat{k} < 1/3$. The estimated values of R_0 are also quite low, and likely biased because the detailed contact tracing data required for this analysis is much more difficult to obtain when disease spread is very rapid. The low values for k, together with relatively low values for R_0, suggest that the great majority of individuals are unlikely to infect any other individual. For example, if $k = 1/3$, then from equation (4.2) it follows that for each individual to have a greater than 50% chance of infecting another individual, R_0 would have to exceed

$$R_0 > \frac{(2)^3 - 1}{3} = 2.33,$$

which is outside the 90% confidence interval for all the datasets analyzed except for smallpox in Europe over the period 1958 to 1973.

Similarly, our methods allow us to estimate that 73% of SARS cases in Singapore were below the critical infectious level of $\nu = 1$, while only 6% had infectiousness of $\nu > 8$ [**51**]. This result is consistent with field reports from SARS-afflicted regions [**48, 66**] indicating that infectiousness is highly overdispersed, but contrasts sharply with many published SARS models that do not take heterogeneity into account (reviewed in [**8**] and [**28**]).

4.2. Characterizing heterogeneity in infectiousness. The dispersion parameter k has little intuitive value as a measure characterizing the heterogeneity of infectiousness among individuals, particularly as the mean infectiousness R_0, expressed in equation (4.1), is not itself independent of k. One way to characterize heterogeneity is to ask what percentage of infectious cases are responsible for a given percentage of all on-going transmission. In a recent publication, Woolhouse et al. [**79**] proposed a general "20/80" rule: 20% of infectious individuals cause 80% of all infections for vector-borne and sexually transmitted diseases. In a homogeneous population the rule would be 20/20 or 80/80.

In general for a heterogeneous population we expect a "$20/P$" rule to arise, where increasing levels of heterogeneity in ν lead to increasing values for P. From

TABLE 1. Parameter estimation and for the Poisson (P), geometric (G) and negative binomial (NB) models of the offspring distribution and statistical support.

Datasets	Model	Akaike weight	$\hat{R}_0$ (90% CI for NB)	$\hat{k}$ (90% CI for NB)	$P\%$ ("$20/P$" rule) (90% CI for NB)
SARS	P	0	1.63	0.16	88%
Singapore 2003	G	0	(0.54,2.65)	(0.11,0.64)	(60,94)
$N = 57$	NB	1			
SARS	P	0	0.94	0.17	87%
Beijing 2003	G	0	(0.27,1.51)	(0.10,0.64)	(60,95)
$N = 33$	NB	1			
Measles	P	0	0.63	0.23	81%
US 1997-9	G	0.01	(0.47,0.80)	(0.13,0.40)	(70,92)
$N = 165$	NB	0.99			
Measles	P	0	0.82	0.21	83%
Canada 1998-2001	G	0.15	(0.72,0.98)	(0.09,0.52)	(44,86)
$N = 49$	NB	0.85			
Smallpox	P	0	3.19	0.37	71%
Europe 1958-73	G	0.02	(1.66,4.62)	(0.26,0.69)	(59,79)
$N = 32^s$	NB	0.98			
Smallpox	P	0	0.80	0.32	74%
Benin 1967	G	0.45	(0.32,1.20)	(0.16,1.76)	(44,88)
$N = 25$	NB	0.55			
Smallpox	P	0	1.49	0.72	58%
W. Pakistan	G	0.71	(*)	(0.32,2.23)	(41,74)
$N = 47$	NB	0.29			
Variola minor	P	0	1.60	0.65	60%
England 1966	G	0.71	(0.88,2.16)	(0.34,2.32)	(41,73)
$N = 25$	NB	0.29			
Monkeypox	P	0	0.32	0.58	62%
Zaire 1980-84	G	0.62	(0.22,0.40)	(0.32,3.57)	(36,74)
$N = 147$	NB	0.37			
Pneumonic plague	P	0	1.32	1.37	0.47%
6 outbreaks	G	0.67	(1.01,1.61)	(0.88,3.53)	(37,54)
$N = 74$	NB	0.33			
Avian influenza	P	0.17	0.06	0.026	100%
S.E. Asia 2004	G	0.32	(0,0.18)	$(0.026,\infty)$	(20,100)
$N = 33$	NB	0.51			
Rubella	P	0	1.00	0.032	100%
Hawaii 1970	G	0	(0.0,1.95)	$(0.013,\infty)$	(20,100)
$N = 19$	NB	1			
Hantavirus	P	0.31	0.70	1.66	45%
Argentina 1996	G	0.52	(0.20,1.05)	$(0.24,\infty)$	(20,80)
$N = 20$	NB	0.17			
Ebola HF	P	0.56	1.50	5.10	34%
Uganda 2000	G	0.28	(0.85,2.08)	$(1.46,\infty)$	(20,46)
$N = 13$	NB	0.17			

*neither the raw data nor a fitted confidence interval were available.

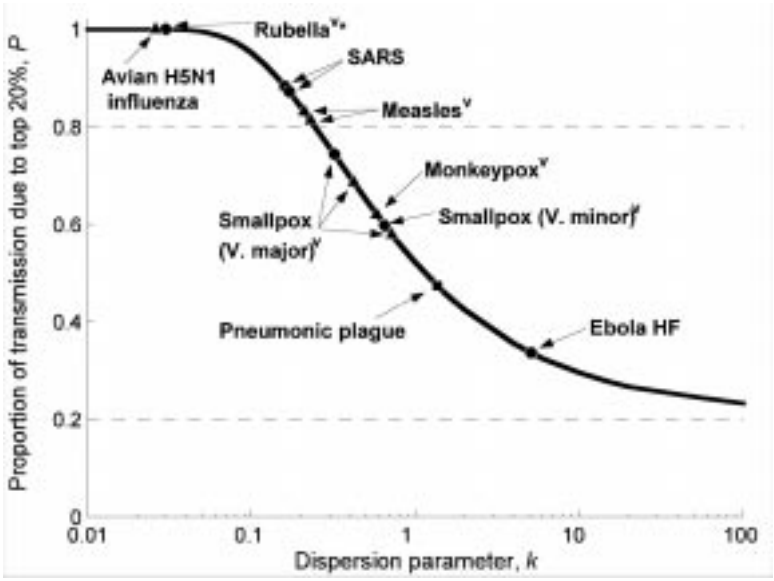

FIGURE 3. Proportion of transmission expected from the most infectious 20% of cases, for data drawn from single outbreaks (circles), multiple outbreaks (squares), and long-term surveillance (triangles). Dashed lines show proportions expected under the 20/80 rule (top) and in a homogeneous population (bottom). Superscripts: v indicates a highly-vaccinated host population; * indicates an outbreak that is probably atypical. See details in Lloyd-Smith et al. [**51**].

the last column in Table 1, we see that "20/80" rule could well be a slight underestimate of the variation observed for SARS, fairly accurate for measles in highly vaccinated populations, and a slight overestimate for smallpox, monkeypox and pneumonic plague. For other diseases broad confidence intervals prevent firm conclusions, but best-fit parameters indicate that the "20/80" rule may seriously underestimate the heterogeneity of infectiousness for H5N1 avian influenza and rubella, and overestimate the heterogeneity for hantavirus and Ebola hemorrhagic fever.

The theory allows us to construct a curve denoting the expected proportion of transmission due to the most infectious 20% of transmitting individuals, as a function of the dispersion parameter of the negative binomial offspring distribution, k. (Of course, 20% is arbitrary and we can construct curves for any percentage we choose.) In Figure 3 such a curve is depicted along with the locations on this curve predicted by best-fit parameters for some of the disease datasets listed in Table 1.

From a technical point of view, particularly when complete contact tracing and construction of a reliable histogram (such as in Figure 2) is difficult to achieve, a crude estimate of the best fitting negative binomial distribution can be obtained from estimates of the mean number of offspring R_0 and proportion q_0 of non-transmitting infected individuals. In this case the value for k is calculated by solving equation (4.2) implicitly using an appropriate numerical method.

In conventional theory for homogeneous populations, R_0 is the only statistic needed to calculate the probability P_{epi} of a major epidemic, as discussed in Section 7 of the previous chapter. The same branching process theory applies to heterogeneous populations, in that the value z_∞ to be used in [**35**, Equation (7.3)] is still the solution to the probability generating function equation $z = g(z)$, but now the probability generating function is for the negative binomial rather than Poisson distribution. Thus z_∞ in this case is the implicit solution of the equation

$$z = \left(1 + \frac{R_0}{k}(1 - z)\right)^{-k}.$$

Using this equation it becomes clear that the probability of a major epidemic is now critically dependent on both k and R_0, and that greater degrees of individual heterogeneity in infectiousness lead to higher probabilities of stochastic extinction in the early phase of disease establishment (Figure 4). Thus, along with R_0, it should be very useful to specify P_{epi} as well. The latter informs us of the probability with which disease will invade the population (i.e. occurrence of an epidemic), while the former informs us on how fast it will spread, if the disease should invade.

4.3. Superspreading events (SSEs) and loads (SSLs). In all epidemics, whether in homogeneous or heterogeneous populations, some infectious cases will not infect any individuals while others will infect many more than the expected number R_0. In heterogeneous populations this greater degree of transmission may arise from biological or social properties of the host individual, while in homogeneous populations it arises from random circumstance; that is, the host individual happens to spend time in close confinement with other individuals (e.g. in a crowded hospital ward or aboard a commuter train) while highly infectious. Occurrences of this kind have been referred to as superspreading events (SSEs) [**48, 49, 62, 66**], even though the individual involved may not have been more infectious than the average infective individual.

Despite numerous published accounts of SSEs in the literature, 37 of which are summarized by Lloyd-Smith et al. [**51**], no coherent approach to their quantitative analysis has emerged until recently. In the case of SARS, for example, using the random variable Z to represent the actual number of individuals infected by a known infectious case, SSEs have been defined as $Z \geq 8$, $Z \geq 10$, $Z > 10$, and "many more than the average number" [**48, 62, 66, 73**]. We propose a general protocol for defining an SSE that scales with the infectiousness of different diseases and naturally incorporates the influence of stochasticity [**51**]. The definition centers on using the Poisson distribution with mean R (where R is the effective reproductive number for the disease and population in question, taking immunization levels into account) as the expected range of Z due to stochasticity in the absence of individual heterogeneity. An SSE is then any case causing more secondary cases than would occur in at least 99% of infectious histories in such a homogeneous population; that is, $Z \geq Z_R^{99}$, where Z_R^{99} is the first integer value for which the cumulative proportion of cases for the Poisson distribution is at least 0.99 (i.e., because the Poisson distribution is discrete Z_R^{99} will, in general, not correspond exactly to the 99^{th} percentile: it is first integer at or beyond this percentile point).

From this definition it follows that in a homogeneous population, at most 1% of infectious cases causes SSEs. From a tabulation of the cumulative Poisson distribution, one finds for example that $Z > 6$ is an SSE when $R = 2$, while an SSE

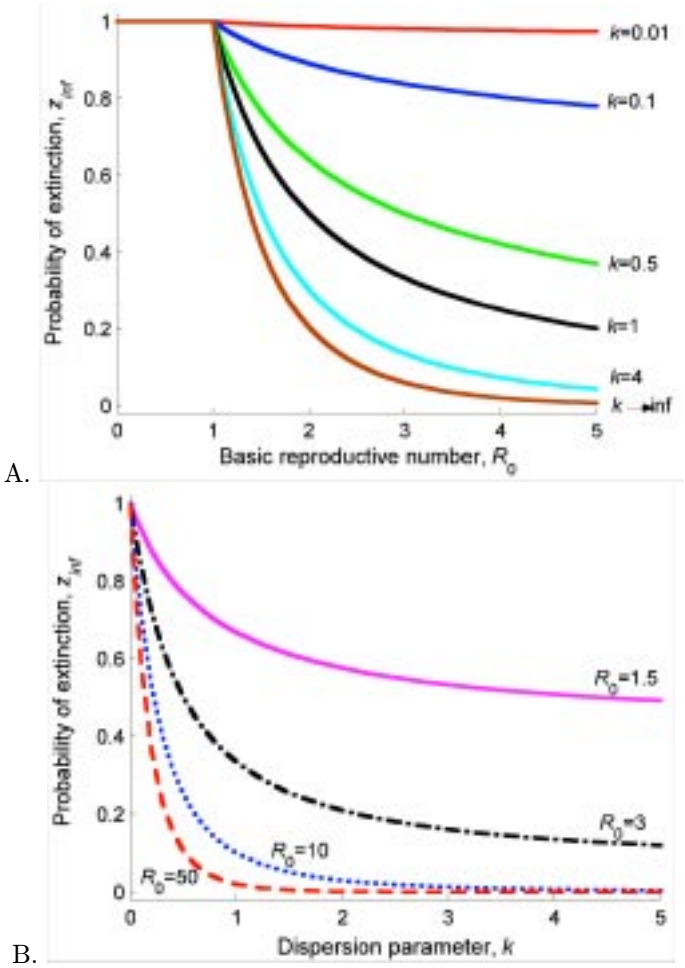

FIGURE 4. Probability of stochastic extinction of an outbreak beginning with a single infectious case for a branching process epidemic with negative binomial offspring distribution (i.e., z_∞, cf. [**35**, Equation (7.3)]). (A) Extinction probability versus population-average reproductive number R_0 for different dispersion parameters k. (B) Extinction probability versus dispersion parameter k for different values of R_0.

for $R = 5$ requires $Z > 11$. In a heterogeneous population, for an epidemic with effective reproductive number R, the tail defined by $Z \geq Z_R^{99}$ will contain an increasing proportion of the population with increasing heterogeneity. We define the magnitude of this increase as the superspreading load (SSL) associated with a heterogeneous population. Specifically, if the tail defined by $Z \geq Z_R^{99}$ contains $r\%$ of events, then we define SSL$= r$. In the context of the negative binomial distribution we can plot the value of SSL as a function of k, as illustrated in Figure 5. In this figure we have selected values of R for which Z_R^{99} defines a tail with precisely 1% of events. As noted above, this is not the case for arbitrary values of R due to the

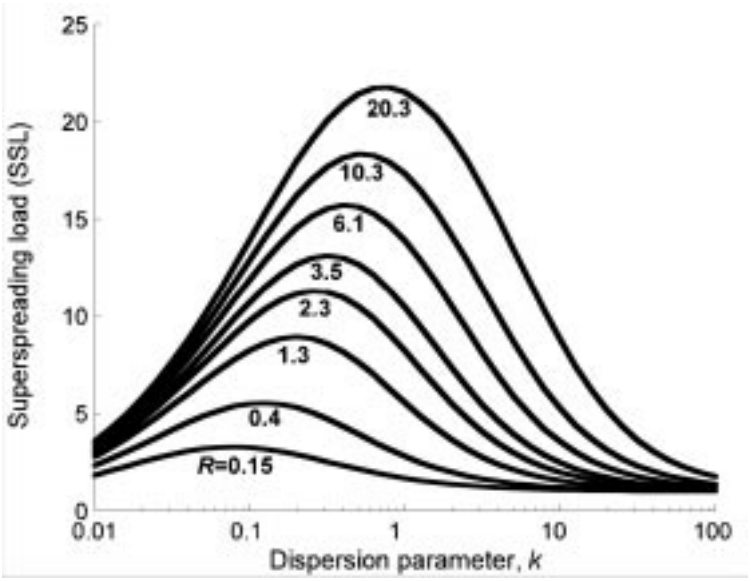

FIGURE 5. Superspreading load (SSL) versus dispersion parameter k for outbreaks with negative binomial offspring distributions. The SSL reflects the percentage of index cases expected to cause 99^{th}-percentile SSEs. Values of R were selected such that $\Pr\{Z \geq Z_R^{99} \mid Z : \text{Poisson}(R)\}$ is precisely 0.01, as described in the text.

discreteness of the Poisson distribution, which will cause discontinuous jumps in SSL as R changes. One way to deal with this problem is to re-define SSL as

$$r = 100\left(\theta\left(\phi_{R,k}^{\text{NB}}\left(Z_R^{99}-1\right)\right) + \sum_{Z=Z_R^{99}}^{\infty}\phi_{R,k}^{\text{NB}}(Z)\right), \tag{4.3}$$

where $\phi_{R,k}^{\text{NB}}(Z)$ is the cdf of the negative binomial distribution, and $0 \leq \theta < 1$ is selected so that in the case of the Poisson ($k \to \infty$) with mean R the value for SSL is precisely 1%. That is, some proportion of the density in the next-lower bin of the Poisson cdf is added to bring SSL to exactly 1%, and the identical proportion of that bin is added when calculated the SSL for negative binomial offspring distributions.

Note from Figure 5 that for R in the range $[1, 20]$, the SSL is maximized when k lies in the range $[0.1, 1]$. In particular, for $R = 6.1$ ($Z_{R=6.1}^{99} = 13$), the SSL is approximately 12 for $k = 0.1$, rises to a maximum of approximately 16 at k around 0.5 and drops again to approximately 14 at $k = 1$. The loads are not quite as severe for lower values of R, but even for the case $R = 1.3$ ($Z_{R=1.3}^{99} = 5$), the SSL rises to a maximum of approximately 9 at k around 0.2. Thus levels of heterogeneity observed in real epidemics (e.g. SARS or smallpox, Table 1) will result in an order of magnitude more SSEs than would be expected if the epidemic were in a population that is homogeneous with respect to infectiousness.

5. Individual-based models in heterogeneous populations

Individual-based models, also referred to as agent-based models or microsimulations, depend on the computational power of computers to represent large numbers of individuals each with their own independent record containing information relevant to the questions being addressed (e.g. age, sex, location, disease status, and so forth). This information is then updated either at stochastically determined times (event driven models) or periodically (discrete time or 'clock-driven' models) (e.g. see [**12**]). The amount of detail that can be put into such models is limited only by the size of the population to be simulated and the power of the computer used to carry out the simulations. Currently, several groups are developing general agent-based modeling software suitable for simulating epidemics in spatially and demographically structure populations (e.g. [**33, 46, 71**]). The three studies outlined in this section used computer programs written in Matlab® and C++ specifically for the problems at hand. The material presented in the first subsection extends our intuition relating to the spread of epidemics in highly idealized populations consisting of n homogeneous groups, initially of size m, linked to each other by migration patterns representing particular spatial configurations. The material presented in the second subsection uses association data obtained from empirical studies to explicitly characterize the contact process when modeling the spread of disease in a population where the movements of each individual are known. Finally, in a third subsection we introduce the question of what happens when a disease invades a host population that is itself invading and colonizing a region, with an illustration on a realistic heterogeneous landscape.

5.1. Epidemics in a group structured population with movement among groups. The formulation in this section is based on the assumption that a population consists of m identifiable subpopulations—a classic metapopulation structure—which is fixed throughout time, but the number of individuals N_i in each subpopulation varies with time and can become 0. In this case, the total population size is $N = \sum_{i=1}^{m} N_i$. The subpopulation in each group is further structured into S and I disease classes. The model reflects two processes: transmission within groups and movement between groups [**64**]. Each group is regarded as being homogeneous with respect to the hazard of transmission, where for the i^{th} group with transmission parameter β_i and frequency-dependent transmission, it follows that the probability that a susceptible in group i will become infected over the interval $[k, k+1]$ is (cf. [**35**, Expression (6.6) and (8.1)])

$$p_{\tau_{ik}} = 1 - \exp\left(-\beta_i \frac{I_i(k)}{N_i(k)}\right).$$

For simplicity, assume that movement between groups is not influenced by the size of any group other than the group from which an individual is departing. Our assumption that the subgroups are homogenous thus implies that any individual in group i has the same probability, $\mu_{ik}(N_i(k))$, of leaving its current group during time step $[k, k+1]$. The group that a departing individual then joins can reflect both spatial (e.g. distance among groups) and recipient group factors (e.g. size of groups). Ways of characterizing these movements have received considerable attention in the ecological literature [**11, 15, 34, 50, 80**], leading to movement matrices of the form considered in Section 3.3, with elements M_{ij} that may depend in relatively complex ways on the group size vector $\mathbf{N} = (n_1 \ldots, n_m)'$. Here we only

consider relatively simple rules that permit us to focus on epidemiological rather than demographic questions.

Cross et al. [**17, 18, 19**] used an individual based model of a metapopulation, structured at the start of the simulation into equally sized groups spatially organized on a square lattice, to investigate the question of how SIR(V) epidemics (recall V is recovered with immunity) depend on relative rates influencing the spread of disease within groups versus the movement of infected individuals among groups. The relative rate of the spread of disease within groups was controlled by the value of a transmission parameter β, which was assumed to be the same in all groups. The relative rate of the spread of disease among groups was controlled by a departure probability parameter μ that was assumed to be the same value for all groups and independent of both time k and departing group size $N_i(k)$.

Three different sets of rules were used to assess the effects of spatial connections on the epidemic in question. First, departing individuals were assumed to move to only one of their four nearest-neighboring groups, each with probability 1/4, and, to avoid boundary effects, opposite edges of the array were connected so that effectively, the population was moving on a torus. Second, individuals were assumed to move with equal probability to one of only two nearest-neighbors, an analysis that is topologically equivalent to populations confined to a one-dimensional loop (e.g. villages located around the circumference of a lake). Third, individuals were permitted to join with equal probability any other group, which is equivalent to an "island" model previously used by Hess [**40**] and Fulford et al. [**34**] to study the spread of disease in metapopulations. Finally, Cross et al. assume that all infected individuals recover to an immune class at a constant probability per time step, $p_\alpha = \alpha$. (Note, p_α is only approximately equal to the recovery rate α when α is small: more precisely $p_\alpha = 1 - e^{-\alpha}$). Although all groups begin in this particular study with the same number of individuals, group sizes do change over the course of simulations. The symmetries within the model with respect to group structure (e.g. lack of boundaries on a torus or loop), however, ensured that group sizes remained relatively equitable during the course of each simulation.

Cross et al. [**17, 18, 19**] compared the dynamics of two diseases with the same R_0 ($\approx \beta/\alpha$ when time steps are relatively small), but one disease was slow with a relatively long infectious period (e.g. $\beta = 0.05$, $\alpha = 0.01$) while the other was an order of magnitude faster (e.g. $\beta = 0.5$, $\alpha = 0.1$). The probability p_μ for an individual to move in one time step was the same for both cases: thus the analysis essentially compares diseases with equal values of R_0 that are fast and slow relative to the time scale of movement. The spread of diseases was compared for four different host population structures varying in levels of heterogeneity: specifically, a single homogeneous group with 1000 individuals, 10 homogeneous groups each of 100 individuals, 25 homogeneous groups each of 40 individuals, and 100 groups each of 10 individuals.

As expected [**40, 77**], the probability of invasion decreases as the population is divided into more smaller groups because the number of intergroup transfers needed for the disease to penetrate the entire population must increase (Figure 6). Also slower diseases are more likely to invade structured populations than faster diseases with the same R_0 because, in the former case, the mean period of infectiousness ($1/\alpha$) is longer, thereby providing more time for inter-group movement of infectious individuals. The simulated epidemics in the single group and 100 group populations

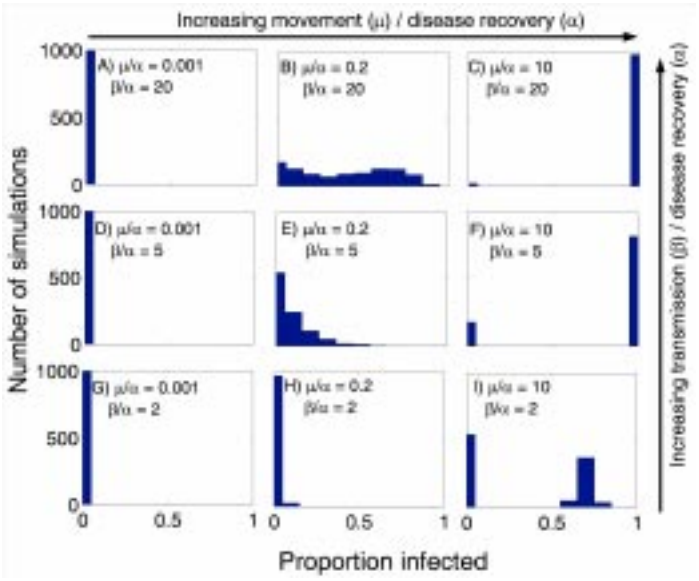

FIGURE 6. Histograms of the proportion of individuals infected during an epidemic for different transmission (β) and movement (μ) values scaled by the probability of disease recovery (α). Each parameter set was simulated 1000 times on an 11×11 toroidal array of groups with 10 individuals each and a recovery probability of 0.1.

were far more similar for the slow than the fast disease. In other words, slow diseases are better approximated by a single homogeneously mixed group than are fast diseases (Figure 7). The mean infectious period ($1/\alpha$) defines the natural disease timescale. When movement occurs on roughly the same timescale or longer, mixing among groups should be modeled mechanistically with explicit host movement (as presented in this and the next subsection) rather than implicitly as a between-group transmission rate that operates simultaneously with within-group transmission.

In socially or spatially structured populations, invasion of disease may depend more on the rate of movement between groups p_μ divided by the mean period of infectiousness than on R_0 itself (where the latter is approximate by the transmission rate β divided by the recovery rate α). In Figure 6, R_0 ($\approx \beta/\alpha$) is 20 for all cases. When p_μ/α is small, however, the disease does not invade the metapopulation. As a rule of thumb, a disease will invade the metapopulation if p_μ/α is greater than the reciprocal of the expected number of individuals that will be infected within a single group [**17, 18, 19**]. This makes intuitive sense because in this model system p_μ/α is the expected number of between-group movements made by each infectious individual. Thus p_μ/α multiplied by the expected number of infected individuals is the expected number of infected dispersers per group, which must exceed 1 for a pandemic to occur. When R_0 is high almost all individuals in a group will be infected. Thus, for a pandemic to occur, p_μ/α should be greater than the reciprocal of the average group size. This rule of thumb, however, also depends upon the average number of neighboring groups. The completely connected topology has a

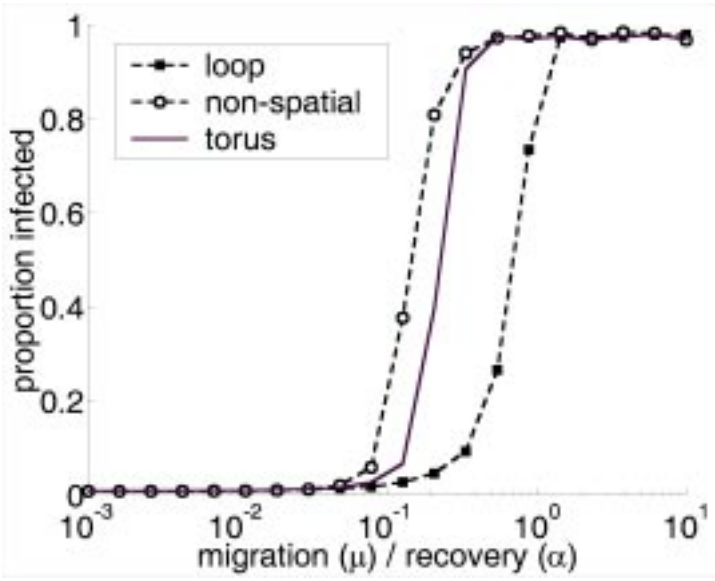

FIGURE 7. The average proportion of the population that becomes infected depends on the spatial configuration: torus, loop, or non-spatial. In the non-spatial array individuals could move to any other group during a single time step. All simulations have 121 groups. Each parameter set was simulated 1000 times, with a group size of 10 and a recovery probability of 0.1.

lower movement to recovery threshold than a more restrictive loop topology (Figure 8).

5.2. Epidemics on dynamic social networks: Populations structured by an association matrix. In Section 5.1 we selected three canonical topologies to describe the movement process in a group structured population. Each of these topologies is an idealization, none of which may fit a particular system very well. Further, in real populations movement is influenced by seasons and space, and movement rates may be time dependent. As a result, individual contacts in real populations are most accurately represented by a dynamic network of social interactions (described in more detail below). Network models provide a much-needed alternative to the assumption of random mixing. Consequently, they have been the focus of much recent research in epidemic theory [**33, 54, 58, 75**]. Network researchers, however, are challenged by depiction of changing social contacts (often resorting to using static, unchanging networks) and by the unavailability of data from which to estimate network parameters.

One approach to these challenges is to apply established methods from studies of animal behavior by constructing an *association matrix* depicting the changing social interactions of all studied individuals [**76**]. A demonstration of this method, discussed below, is a study reported by Cross et al. [**16**]) on the spread of disease in an African buffalo population in the Kruger National Park, South Africa. We tracked buffalo with radio collars for a two-year period, noting how often different individuals were seen together in the same herd. These data were then used to

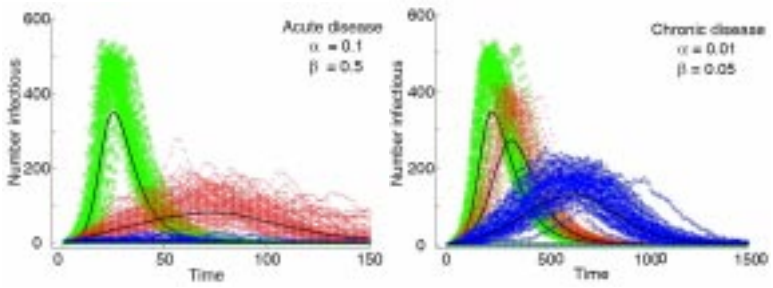

FIGURE 8. Disease invasion depends upon population structure (green circles: 1 group of 1000 individuals; red points: 25 groups of 40 individuals; blue crosses: 100 groups of 10 individuals) and the duration of the infectious period. A mean-field model of one group is a worse approximation for an acute disease with $\alpha = 0.1$ (left panel) than a chronic disease with $\alpha = 0.01$ (right panel). For both diseases $\beta/\alpha = 5$, but the slow disease is more likely to invade the structured population. Lines represent the mean of 100 simulations with frequency-dependent transmission and 1000 individuals. Simulations with 25 or 100 groups were run on a toroidal spatial structure with a movement probability μ of 0.01.

construct a time-dependent set of association matrices $\mathbf{A}(k)$ with entries $a_{ij}(k)$ that represent the proportion of time individuals i and j (dyad i-j) spent together (i.e. were located in the same herd) over the k^{th} time interval $[k-1, k]$, $k = 1, \ldots, T$ (Cross et al. [**17, 18, 19**], Szykman et al. [**69**], Whitehead [**76**], Wittemyer et al. [**78**]).

Assuming that association indices $a_{ij}(k)$ for all dyads in the population have been measured, the matrices $\mathbf{A}(k)$, $k = 1, \ldots, T$, can be used in an individual-based model to investigate how a disease introduced at time $t = 0$ into this population might spread through it. Specifically, let the vector $X_i(k) = \binom{a}{b}$, $a, b = 0$ or 1, represent the disease state of individual i at time k, where $x_i(k)' = (0,0)$, $(1,0)$ and $(0,1)$ ($'$ is the transpose of the vector) respectively represent a susceptible, infected, and recovered individual at time t. Then over a time interval $[0, T]$, every individual that becomes infected has a profile of the form

$$\begin{array}{ll} X_i(l) = (0,0)' \ (S \text{ class}) & l = 0, \ldots, k_1 - 1 \leq T \\ X_i(l) = (1,0)' \ (I \text{ class}) & l = k_1, \ldots, k_2 - 1 \leq T \text{ provided } k_1 \leq T \\ X_i(l) = (0,1)' \ (R \text{ class}) & l = k_2, \ldots, T \text{ provided } k_2 \leq T, \end{array} \tag{5.1}$$

where k_1 and k_2 are the points in time where the individual made the transition from $S \to I$ and $I \to R$ respectively. Thus summing over the first and second entries for each individual at time k immediately tells us how many individuals are infected and how many removed at time k. Now assume that the hazard rate for the transmission of disease between an infected individual j and a susceptible individual i, $i, j = 1, \ldots, N$, is determined by a common underlying transmission coefficient β multiplied by the association coefficient $a_{ij}(k)$ (recall that $a_{ij}(k)$ is an estimate of the proportion of time individuals i and j spent together over the period $[k-1, k]$.)

These pairwise transmission hazards are then summed over all j to obtain the total hazard rate for susceptible i. Additionally, assume that infected individuals enter a V class at a rate α independent of time. Under these assumptions, recalling [**35**, Expressions (6.6) and (8.1)], the probabilities of infection and recovery take the form (note the use of vector dot product in the first expression):

$$p_{i\tau_k} = 1 - e^{-\beta \sum_{j=1}^{n} a_{ij}(k)((1,0)\cdot X_j(k))}, \quad k = 0, 1, 2, \ldots, T-1, \tag{5.2}$$
$$p_\alpha = 1 - e^{-\alpha}.$$

Note that the i^{th} individual's probability of infection differs from other individuals because the i^{th} individual has its own set of association coefficients $\{a_{ij}(k), j = 1, \ldots, N\}$. This approach essentially elaborates the average contact rate in a mass action expression of transmission with individual level details (the association matrix $\mathbf{A}(k)$ with elements $(\mathbf{A}(k))_{ij} = a_{ij}(k)$, $i, j = 1, \ldots, N$, determines the actual contact rates for each individual).

In most cases, the number of individuals monitored to obtain the association matrix $\mathbf{A}$ is only a small fraction of the population, perhaps as low as 5%. Thus the question in the context of individual-based models is how to statistically create the other 95% of individuals in the population by scaling up the matrix $\mathbf{A}$ from N^2 to $(20N)^2$ entries, while retaining the emergent group structures (i.e. herd structure in the case of African buffalo) evident in the sampled subset of the population. A quick and dirty solution in the case of a 5% sampling is to assume that the every individual would have 20 times more contacts than indicated by the matrix $\mathbf{A}$ arising from the sample; in which case, we might simply assume that

$$p_{i\tau_k} = 1 - e^{-20\beta \sum_{j=1}^{n} a_{ij}(k)((1,0)\cdot X_j(k))}.$$

This simplification is adequate when the number of infected individuals is relatively large, but not for invasion analysis. In this latter case, introducing one infective into the model is not equivalent to introducing 20 infectives into the population because the effects of demographic stochasticity cannot simply be scaled up. Further, this kind of scaling ignores the network correlations between infected individuals that inevitably build up in the early stages of disease invasion [**45**]. If we are only interested in a comparative analysis, however, of the course of an epidemic for different values of β and α that constitute the same ratio $R_0 = \beta/\alpha$, then an individual based simulation using an association matrix constructed from a population sample provided some insights into the effects of the relative differences in the disease and movement time scales on epidemics.

Associated with every $N \times N$ matrix $\mathbf{A}(k)$ is a network of N nodes, where the i^{th} and j^{th} nodes are connected at time k if and only if $a_{ij} > 0$. The importance of this network topology on the spread of disease can be investigated by randomly rewiring a proportion δ of all connections to obtain versions of the matrices $\mathbf{A}(k)$ that represent the same number of connections. Any non-random group structure inherent in the topology at time k would be progressively destroyed as δ increased from 0 to 1. In particular, randomizing all connections ($\delta = 1$) destroys all group structures while preserving the average degree of connectedness of the network. Two types of rewiring simulations can be conducted. In *static rewiring* simulations, a proportion δ of the connections are rewired at the beginning of the simulation with the same reorganized matrix used throughout the rest of the simulation. In *dynamic*

rewiring simulations, in each time step a proportion δ of the connections of $\mathbf{A}$ used in the previous time step are rewired so that even for small δ the matrix $\mathbf{A}$ becomes progressively more randomized over the course of the simulation. (Examples of these two procedures are shown below.)

The importance of variation in connection frequency or strength across the values $a_{ij}(k)$, $k = 1, \ldots, T$, obtained for each dyad i-j, $i, j = 1, \ldots, N$, can also be investigated by increasing the variance over time while keeping the time-averaged association value $\bar{a}_{ij} = \sum_{k=1}^{T} a_{ij}(k)$ among dyads constant. High variance among a_{ij} values corresponds to situations where individuals have two sets of associates, those that they spend most of their time with and those that they rarely encounter. Low variance implies a well-mixed population. One might hypothesize that weak connections are less significant for disease transmission, and hence that systems with a high variance in connection strength may be less permeable to disease spread. On the other hand, the disease may spread more rapidly amongst those individuals that are tightly associated.

The variance can be manipulated while preserving the mean of the associations of each dyad i-j by defining a new set of elements a_{ij}^{γ} of an association matrix $\mathbf{A}^{\gamma}$ modified using the following algorithm: a value z of a uniformly distributed random variable Z on $[0, 1]$ is drawn and then

$$a_{ij}^{\gamma} = \begin{cases} \bar{a}_{ij} + \gamma(1 - \bar{a}_{ij}) & \text{if } \bar{a}_{ij} > z \\ \bar{a}_{ij} - \gamma(\bar{a}_{ij}) & \text{otherwise} \end{cases}$$

is calculated with the process repeated for each $i, j = 1, \ldots, N$. Clearly, for the extreme cases $\gamma = 0$ and 1, this procedure produces $a_{ij}^{0} = \bar{a}_{ij}$ and $a_{ij}^{1} = 0$ or 1. Note that the algorithm preserves the topology of the connections except when $\alpha = 1$, when some connections are entirely removed and the total proportion of connections is reduced to $\bar{a}_{ij}$.

Cross et al. [**16**] applied the above methods to association data obtained for African buffalo from multi-week observations over a two-year period. From these data, they constructed 24 monthly association matrices for 64 individuals. The networks associated with May 2002 and the entire study period are illustrated in Figure 9. These 24 matrices were then used to investigate questions regarding the spread of disease in this population. Repeating the sequence of 24 association matrices twice (i.e. $\mathbf{A}(24 + k) = \mathbf{A}(k)$, $k = 1, \ldots, 24$) to construct a 48 month period, Cross et al. simulated the spread of a slow moving ($\beta = 0.4$, $\alpha = 0.3$) and a fast moving ($\beta = 0.04$, $\alpha = 0.03$) SIR disease (Figure 10). Note that both epidemics have the same basic reproductive number $R_0 = 4/3$, so that any differences that arise between sets of simulations of epidemics are due to time scale differences in the disease dynamics (the first is ten times faster than the second) relative to the rate of mixing as determined by the association matrices. These simulations indicate that a faster-moving disease is more likely to fade out than a slower-moving disease because the latter integrates over a longer time period; and, the longer the time period of integration, the more likely it becomes that any two individuals make contact (i.e. the underlying contact network becomes more fully connected). These simulations based on empirical social networks thus yield conclusions regarding timescales that are consistent with findings presented in Section 5.1 for an idealized metapopulation.

Cross et al. [**16**] also showed, using the same association matrix at each timestep (specifically, buffalo data from November 2001) that partial random rewiring had a

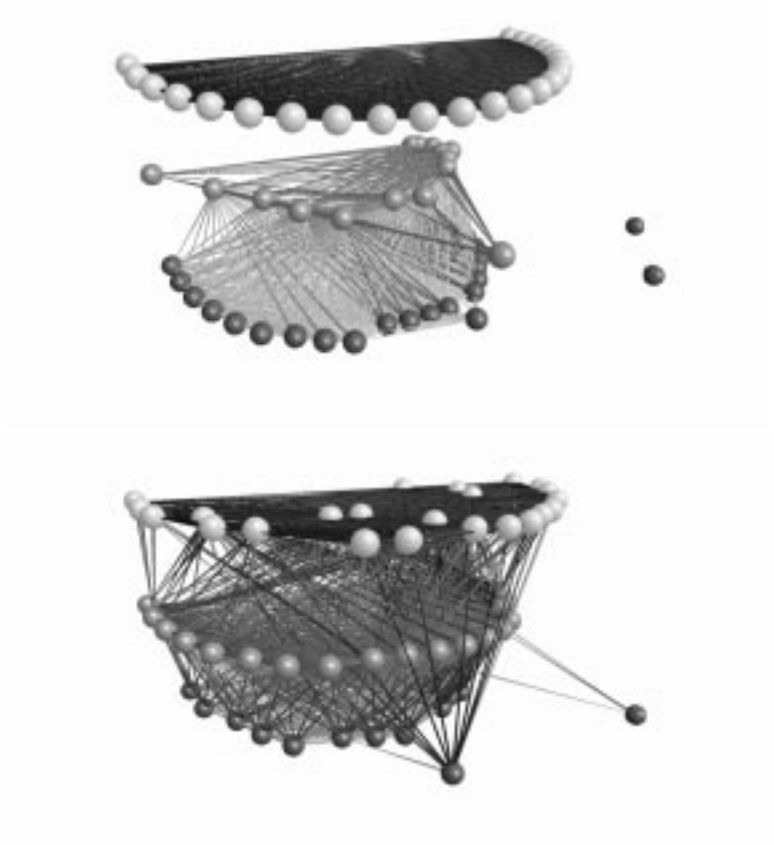

FIGURE 9. Network graphs of the buffalo association data for May 2002 (A) and November 2001 through October 2003 (B). Balls represent individual buffalo and the lines represent all non-zero association values. Individuals are distributed vertically according to herd membership, which was determined by UPGMA cluster analysis.

non-linear effect upon disease dynamics. In Figure 11 we see that small increases in the proportion δ of nodes rewired randomly at each step (i.e. the dynamic rewiring simulation described above) lead to solutions that rapidly approach those of a completely random network ($\delta = 1.0$) by the time $\delta = 0.2$.

Finally, Cross et al. found that variance in the connection strength among dyads had a substantial effect only under certain circumstances. Using the same association matrix at each timestep, they found that increasing the variance (i.e. increasing the value of the parameter γ) had less effect upon slower than faster diseases. Further, increasing variance had little effect when the particular association matrix used in the simulation represented either a very well or very weakly connected group of individuals. This effect was investigated further in association matrices made more sparse by dropping a proportion of connections at random from an empirical association matrix at the beginning of the simulation. Reducing the

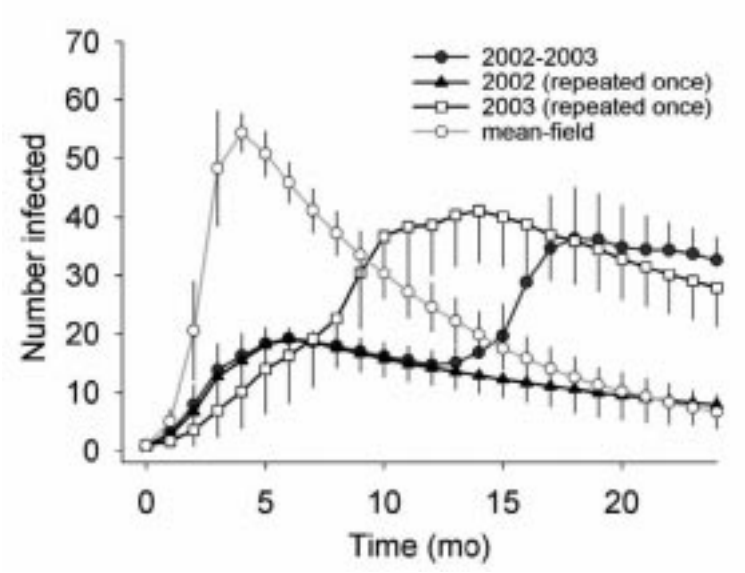

FIGURE 10. Mean and standard deviations (over 50 stochastic simulations) of the number of infected individuals using monthly association data from the entire study period (closed circles), 2002 (closed triangles), 2003 (open squares), or a mean-field model (open circles). All simulations used a transmission coefficient β of 0.3 and recovery probability γ of 0.1. For simulations using one year of data, the same association matrices were used again the second year.

number of connections between individuals had a relatively large impact compared with the effect of increasing the variance in connection strength (Figure 12).

5.3. Epidemics in colonizing populations. Our final example considers the spread of disease in a population that is itself expanding over a given landscape. The particular setting for this problem pertains to the reintroduction of Persian fallow deer (*Dama mesopotamica*) in northern Israel [**6**] and the assessment of how this reintroduction might have been affected if one of the founding individuals had been infected with a transmissible disease [**7**]. A disease of potential concern for Persian fallow deer is bovine tuberculosis (BTB), which occurs in the European fallow deer, *Dama dama* [**3, 56**]. BTB is endemic in wildlife species such as brushtail possums, badgers, African buffalo and white-tailed deer in numerous countries worldwide, with serious economic, ecological and public health consequences [**59**]. Therefore it is essential to understand the basic processes underlying its possible spread in this reintroduced species, and in evaluating the potential efficacy of different management strategies should BTB be detected in the northern Israel Persian fallow deer population. We have undertaken such an evaluation using a range of parameter values that have been measured with regard to the transmission of BTB in other deer populations (unfortunately all captive, though—see Wahlström et al. [**74**]).

In a homogeneous landscape, simple models predict that a colonizing host population will spread out in a radially symmetric fashion, with a wavefront that has

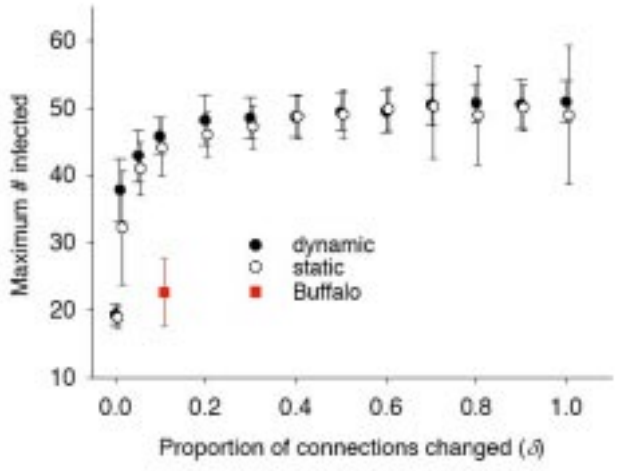

FIGURE 11. The maximum number of individuals infected at any point in time after 50 time steps depends upon the amount δ of random rewiring of the association network at the beginning of each simulation (static) or cumulatively every time-step (dynamic). Dynamic and static simulations started with association data from November 2001; the point pertaining to the buffalo data was generated using all of the association data (i.e. unmanipulated). Disease parameters were $\beta = 0.3$, $\alpha = 0.2$. Error bars represent the standard deviations from 50 stochastic simulations. (For clarity, δ values of the static simulations were increased slightly before plotting.)

a characteristic velocity $V_p(t)$ [**67**]. Depending on details of the population's dispersal process, this velocity may be constant or increase with time [**47, 55**] until the population runs out of space to expand. The rate at which disease spreads in a colonizing population obviously depends on the value of R_0 for that disease (as would be measured in population that has a relatively large number of susceptibles). From the material that has been presented thus far, we expect that the disease will fade out unless R_0 is comfortably above 1. If the disease invades successfully, it can also be regarded as a colonizing process that in a homogeneous population has its own radially expanding wavefront with velocity $V_d(t)$ [**55**].

In a homogeneous population we expect the following three scenarios [**7**]: 1.) The disease fades out if R_0 is less than or equal to 1, or fades out with high probability if R_0 is slightly greater than 1; 2.) If $V_d(t) < V_p(t)$ for all t during the population colonization phase, then the disease wavefront lags behind the population wavefront and the disease only pervades the entire population some time after the population runs out of space; 3.) If $V_d(t) > V_p(t)$ during the initial phase of the disease, then the disease wavefront follows close behind the population wavefront until colonization is complete.

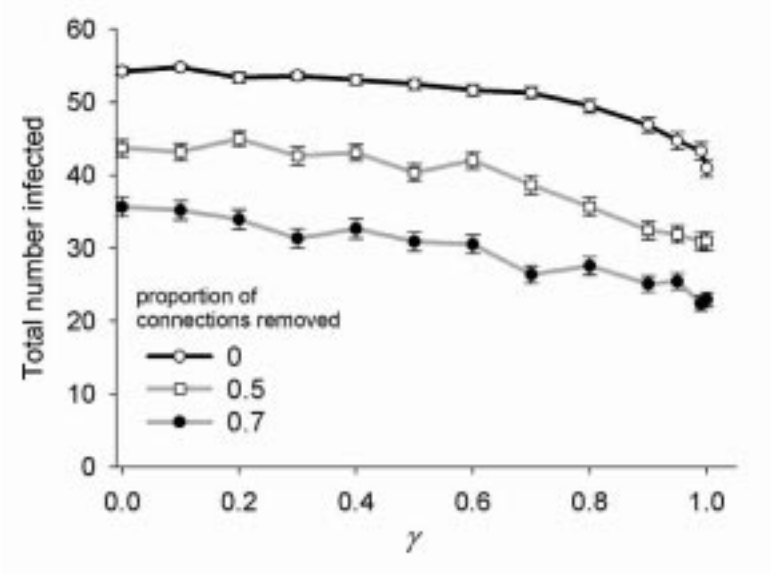

FIGURE 12. The total number of individuals infected after 50 time-steps decreases with increasing variability in the time-averaged connection strength between pairs and decreasing temporal variability of connections within pairs (γ) and the proportion of connections that are removed from the network. See the text for a description of how γ increases the variance in association indices. Error bars indicate the standard errors of 200 simulations using September 2003 as the association matrix, $\beta = 0.3$, and $\alpha = 0.1$.

Here we illustrate these three possible outcomes for the situation of Persian fallow deer colonizing a heterogeneous landscape. The model is run on a GIS landscape template that maps a 630 km^2 region of northern Israel into 300×213 1-hectare pixel elements, each of which has been rated with respect to its quality as fallow deer habitat. Details of how animals move around and establish territories are given elsewhere [**6**]. Transmission is modeled by assuming that individuals make contact with other individuals in proportion to the degree to which their respective home ranges overlap [**60**]. Individuals are assumed to have a fixed time budget for interaction with other deer (cf. the density-independent contact rate of frequency-dependent transmission), so the hazard rate of infection scales with the proportion of all territory overlaps that are occupied by infectious deer (rather than the total overlap, which would correspond to mass-action transmission with density- dependent contact rates).

To implement this assumption, the area of overlap a_{ij} for any two individuals i and j needs to be calculated, after which in the notation of expression (5.1) and the following frequency dependent analog of equation (5.2) can be applied to calculate the probability that any individual in the model contracts the disease over a given period of time:

$$p_{i\tau_k} = 1 - e^{-\beta \left(\sum_{j=1}^{n} a_{ij}(k)((1,0)\cdot X_j(k)) \right) \Big/ \sum_{j=1}^{n} a_{ij}(k)}$$

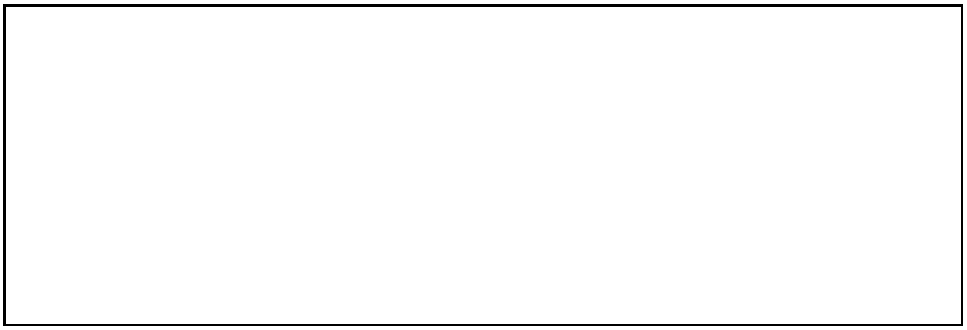

FIGURE 13. Host population density (black) and disease prevalence (purple) are plotted at the end of 10 year projections from onset of the reintroduction of deer into northern Israel (one infected individual at start or reintroduction), for the cases A. $\beta = 0.1$, B. $\beta = 0.5$, C. $\beta = 1$ and D. $\beta = 0.5$ with vaccination (100% effective with life-long protection in all released individuals from the third year onwards and all wild-born young). Results are averaged over 250 simulations runs, and pixels were colored if their average density of host individuals (black) or infected individuals (purple) over all runs was at least 0.5.

In stochastic simulations of the model, the heterogeneous landscape affects the pattern of the frontal wave of the population expansions, and induces the establishment of population activity centers in preferred habitats [**6, 7**] and disease centers within them. The disease range expansion within the colonizing population follows patterns similar to our predictions for a homogeneous landscape: the transmission coefficient values (β) have a major effect on the velocity of disease expansion and the distance at which it follows the range expansion of the population (Figure 13a–c). When β is low, unsurprisingly, the disease has a high probability of fading out of the population, even without any management interventions (Figure 13a).

For cases in which intervention efforts are needed, simulations of such a model may help managers to set targets and predict management outcomes (Figure 13d). Field tests in which host individuals are examined for their disease status along transects radiating outward from the introduction site are important to ascertain the relative positions of the disease and population wavefronts. This information will help managers to distinguish between the three idealized scenarios described above, and to evaluate the management options aimed at containing the spread of disease.

6. Conclusion

In this chapter, we have provided a synthetic overview of connections among the various models we have used to address a range of theoretical and applied problems, by showing how they are outgrowths of canonical deterministic and branching

process SIR methods. Along the way, we have endeavoured to emphasize new properties that emerge as one moves beyond the structurally homogeneous theory into the more realistic world of heterogeneity with regard to demographic, epidemiologic, behavioural and spatial structure.

From the material we present, it is clear that assumptions of homogeneity oversimplify the analysis of most epidemics to the point where estimates of R_0 alone do not adequately describe disease dynamics. Heterogeneity has a profound effect on epidemics and ignoring it leads to substantial bias in estimating the probability with which a disease will invade (Figure 4) or the proportion of individuals that will ultimately become infected (Figure 6). This is why it is important to characterize a disease in heterogeneous populations using appropriate measures, such as R_0 and P_{epi} (cf. [**35**, Equation (7.3)]) when heterogeneity exists with regard to the rates at which diseases are transmitted from one individual to another or, in the case of metapopulations, group size and relative time-scales of movement and transmission/demographic processes.

Much work remains to be done to provide a more coherent theory on the spread of disease in heterogeneous populations. Of course, it will be difficult to generalize the effects that the idiosyncratic spatial structures found in all real systems will have on epidemics. Other more generally defined processes, however, such as time scale relationships in canonical metapopulation formulations, or descriptions of heterogeneity using negative binomial, gamma, or other well-known distributions, provide opportunities for gaining new insights into the spread and control of disease in heterogeneous populations.

Acknowledgements

Grants to WMG from the NSF/NIH Ecology of Infectious Disease Program (DEB-0090323), NIH-NIDA (R01-DA10135), and the James S. McDonnell Foundation 21st Century Science Initiative supported various components of the research reported in this chapter. We thank Alison Galvani and an anonymous reviewer for comments that have lead to improvements of this chapter.

References

[1] L. Aaron, D. Saadoun, I. Calatroni, O. Launay, N. Memain, V. Vincent, G. Marchal, B. Dupont, O. Bouchaud, D. Valeyre, and O. Lortholary, Tuberculosis in HIV-infected patients: a comprehensive review, *Clinical Microbiology and Infection* **10** (2004), 388–398.

[2] R. M. Anderson and R. M. May, *Infectious Diseases of Humans: Dynamics and Control*, Oxford University Press, Oxford, 1991.

[3] A. Aranaz, L. de Juan, N. Montero, C. Sanchez, M. Galka, C. Delso, J. Alvarez, B. Romero, J. Bezos, A. I. Vela, V. Briones, A. Mateos, and L. Dominguez, Bovine tuberculosis (Mycobacterium bovis) in wildlife in Spain, *Journal of Clinical Microbiology* **42** (2004), 2602–2608.

[4] M. Badri, R. Ehrlich, R. Wood, T. Pulerwitz, and G. Maartens, Association between tuberculosis and HIV disease progression in a high tuberculosis prevalence area, *International Journal of Tuberculosis and Lung Disease* **5** (2001), 225–232.

[5] F. Ball and O. D. Lyne, Stochastic multi-type SIR epidemics among a population partitioned into households, *Adv. Appl. Prob.* **33** (2001), 99–123.

[6] S. Bar-David, D. Saltz, and T. Dayan, Predicting the spatial dynamics of reintroduced populations—the Persian fallow deer, *Ecological Applications*, in press, 2005.

[7] S. Bar-David, . O. Lloyd-Smith, and W. M. Getz, Infectious disease in colonizing populations: simultaneous expansion processes and implications for conservation, in review, 2005.

[8] C. T. Bauch, J. O. Lloyd-Smith, M. Coffee, and A. P. Galvani, Dynamically modeling SARS and respiratory EIDs: past, present, future, *Epidemiology* (2005).

[9] S. M. Blower, P. M. Small, and P.C. Hopewell, Control strategies for tuberculosis epidemics: new models for old problems, *Science* **273** (1996), 497–500.
[10] S. M. Blower and T. Chou, Modeling the emergence of 'hot zones': tuberculosis and the amplification dynamics of drug resistance, *Nature Med.* **10** (2004), 1111–1116.
[11] J. M. Bossenbroek, C. E. Kraft, and J. C. Nekola, Prediction of long-distance dispersal using gravity-models: Zebra mussel invasion of inland lakes, *Ecol. Appl.* **11** (2001), 1778–1788.
[12] P. Bratley, B. L. Fox, and L. E. Schrage, *A Guide to Simulation*, Springer-Verlag, New York, 1987.
[13] K. P. Burnham and D. R. Anderson, *Model Selection and Inference: a Practical Information-Theoretic Approach*, Springer-Verlag, New York, 1998.
[14] A. D. Cliff and P. Haggett, Disease diffusion: The spread of epidemics as a spatial process, in (M. Pacione, ed.), *Medical Geography: Progress and Prospect*, Croom Helm., London, 1986.
[15] J. Clobert, E. Danchin, A. A. Dhondt, and J. D. Nichols, eds., *Dispersal*, Oxford University Press, Oxford, UK, 2001.
[16] P. C. Cross, J. O Lloyd-Smith, J. Bowers, C. T. Hay, M. Hofmeyr, and W. M. Getz, Integrating association and disease dynamics: an illustration using African buffalo data, *Annals Zoologici Fennici* **41** (2004), 879–892.
[17] P. C. Cross and W. M. Getz, Assessing vaccination as a control strategy in an ongoing epidemic: Bovine Tuberculosis in African buffalo, *Ecological Modelling*, in review, 2005.
[18] P. C. Cross, J. O Lloyd-Smith, and W. M. Getz, Disentangling association patters in fission-fusion societies using African buffalo as an example, *Animal Behavior* **69** (2005), 499–506.
[19] P. C. Cross, J. O. Lloyd-Smith, P. L. Johnson, and W. M. Getz, Dueling time scales of host mixing and disease recovery determine invasion of disease in structured populations, *Ecology Letters*, in press, 2005.
[20] E. L. Corbett, C. J. Watt, N. Walker, D. Maher, B. G. Williams, M. C. Raviglione, and C. Dye, The growing burden of tuberculosis: global trends and interactions with the HIV epidemic, *Arch Intern Med* **163** (2003), 1009–1021.
[21] M. Cruciani, M. Malena, O. Bosco, G. Gatti, and G. Serpelloni, The impact of human immunodeficiency virus type 1 on infectiousness of tuberculosis: a meta-analysis, *Clin Infect Dis* **33** (2001), 1922–1930.
[22] C. S. Currie, B. G. Williams, R. C. Cheng, and C. Dye, Tuberculosis epidemics driven by HIV: is prevention better than cure?, *AIDS* **17** (2003), 2501–2508.
[23] P. D. Davies, The role of DOTS in tuberculosis treatment and control, *Am J Respir Med* **2** (2003), 203–209.
[24] J. H. Day, A. D. Grant, K. L. Fielding, L. Morris, V. Moloi, S. Charalambous, A. J. Puren, R. E. Chaisson, K. M. De Cock, R. J. Hayes, and G. J. Churchyard, Does tuberculosis increase HIV load?, *Journal of Infectious Diseases* **190** (2004), 1677–1684.
[25] O. Diekmann, J. A. P. Heesterbeek, and J. A. J. Metz, On the definition and computation of the basic reproduction ratio R_0 in models for infectious diseases in heterogeneous populations, *Journal of Mathematical Biology* **28** (1990), 365–382.
[26] O. Diekmann and J. A. P. Heesterbeek, *Mathematical Epidemiology of Infectious Diseases: Model Building, Analysis, and Interpretation*, Chichester, Wiley, New York, 2000.
[27] K. Dietz and K. P. Hadeler, Epidemiological models for sexually transmitted disease, *Journal of Mathematical Biology* **26** (1988), 1–25.
[28] C. A. Donnelly, A. C. Ghani, G. M. Leung, A. J. Hedley, C. Fraser, S. Riley, L. J. Abu-Raddad, L. M. Ho, T. Q. Thach, P. Chau, K. P. Chan, T. H. Lam, L. Y. Tse, T. Tsang, S. H. Liu, J. H. B. Kong, E. M. C. Lau, N. M. Ferguson, and R. M. Anderson, Epidemiological determinants of spread of causal agent of severe acute respiratory syndrome in Hong Kong, *Lancet* **361** (2003), 1761–1766.
[29] C. Dye, G. P. Garnett, K. Sleeman, and B. G. Williams, Prospects for worldwide tuberculosis control under the WHO DOTS strategy. Directly observed short-course therapy, *Lancet* **352** (1998), 1886–1891.
[30] C. Dye, C. J. Watt, and D. Bleed, Low access to a highly effective therapy: a challenge for international tuberculosis control, *Bulletin of the World Health Organization* **80** (2002), 437–444.
[31] C. Dye, C. J. Watt, D. M. Bleed, and B. G. Williams, What is the limit to case detection under the DOTS strategy for tuberculosis control?, *Tuberculosis* **83** (2003), 35–43.

[32] B. Efron and R. J. Tibshirani, *An introduction to the bootstrap*, Chapman and Hall, London, 1993.
[33] S. Eubank, H. Guclu, V. S. A. Kumar, M. V. Marathe, A. Srinivasan, Z. Toroczkai, and N. Wang, Modelling disease outbreaks in realistic urban social networks, *Nature* **429** (2004), 180–184.
[34] G. R. Fulford, M. G. Roberts and J. A. P. Heesterbeek, The metapopulation dynamics of an infectious disease: Tuberculosis in possums, *Theor. Popul. Biol.* **61** (2002), 15–29.
[35] W. M. Getz and J. O. Lloyd-Smith, Basic methods for modeling the invasion and spread of contagious diseases, this volume.
[36] B. Grenfell and J. Harwood, (Meta)population dynamics of infectious diseases, *Trends Ecol. Evol.* **12** (1997), 395–404.
[37] K. P. Hadeler and C. Castillo-Chavez, A core group model for disease transmission, *Math. Biosci.* **128** (1995), 41–55.
[38] T. J. Hagenaars, C. A. Donnelly, and N. M. Ferguson, Spatial heterogeneity and the persistence of infectious disease, *J. theoret. Biol.* **229** (2004), 349–359.
[39] J. A. P. Heesterbeek, A brief history of R-0 and a recipe for its calculation, *Acta Biotheor.* **50** (2002), 189–204.
[40] G. Hess, Disease in metapopulation models: Implications for conservation, *Ecology* **77** (1996), 1617–1632.
[41] C. B. Holmes, E. Losina, R. P. Walensky, Y. Yazdanpanah, and K. A. Freedberg, Review of Human Immunodeficiency Virus Type 1-Related Opportunistic infections in Sub-Saharan Africa, *Clin. Inf. Dis.* **36** (2003), 652–662.
[42] Y. H. Hsieh and S. P. Sheu, The effect of density-dependent treatment and behavior change on the dynamics of HIV transmission, *J. Math. Biol.* **43** (2001), 69–80.
[43] J. M. Hyman and J. Li, Behavior changes in SIS STD models with selective mixing, *SIAM J. Appl. Math.* **57** (1997), 1082–1094.
[44] J. E. Kaplan, D. Hanson, M. S. Dworkin, T. Frederick, J. Bertolli, M. L. Lindegren, S. Holmberg, and J. L. Jones, Epidemiology of human immunodeficiency virus-associated opportunistic infections in the United States in the era of highly active antiretroviral therapy, *Clin Infect Dis.* **30** (2000), S5–14.
[45] M. J. Keeling, The effects of local spatial structure on epidemiological invasions, *Proceedings of the Royal Society of London Series B-Biological Sciences* **266** (1999), 859–867.
[46] E. L. Korenromp, R. Bakker, S. J. de Vlas, R. H. Gray, M. J. Wawer, D. Serwadda, N. K. Sewankambo, and J. D. F. Habbema, HIV dynamics and behaviour change as determinants of the impact of sexually transmitted disease treatment on HIV transmission in the context of the Rakai trial, *AIDS* **16** (2002), 2209–2218.
[47] M. Kot, M. A. Lewis, and P. van den Driessche, Dispersal data and the spread of invading organisms, *Ecology* **77** (1996), 2027–2042.
[48] Y. S. Leo, M. Chen, B. H. Heng, C. C. Lee, N. Paton, B. Ang, P. Choo, S. W. Lim, A. E. Ling, M. L. Ling, B. K. Tay, P. A. Tambyah, Y. T. Lim, G. Gopalakrishna, S. Ma, L. James, P. L. Ooi, S. Lim, K. T. Goh, S. K. Chew, and C. C. Tan, Severe acute respiratory syndrome – Singapore, 2003, *Morbidity and Mortality Weekly Report* **52** (2003), 405–411.
[49] M. Lipsitch, T. Cohen, B. Cooper, J. M. Robins, S. Ma, L. James, G. Gopalakrishna, S. K. Chew, C. C. Tan, M. H. Samore, D. Fisman, and M. Murray, Transmission dynamics and control of severe acute respiratory syndrome, *Science* **300** (2003), 1966–1970.
[50] J. O. Lloyd-Smith, Scaling of resource-driven density dependence in heterogeneous landscapes: dispersal as a case study, *Ecology* (2005).
[51] J. O. Lloyd-Smith, S. J. Schreiber, P. E. Kopp, and W. M. Getz, Superpreading and the impact of individual variation on disease emergence, *Nature*, in review, 2005.
[52] L. G. Louie, W. E. Hartogensis, R. P. Jackman, K. A. Schultz, L. S. Zijenah, C. H. Y. Yiu, V. D. Nguyen, M. Y. Sohsman, D. K. Katzenstein, and P. R. Mason, Mycobacterium tuberculosis/HIV-1 coinfection and disease: Role of human leukocyte antigen variation, *Journal of Infectious Diseases* **189** (2004), 1084–1090.
[53] E. Mañas, F. Pulido, J. M. Pena, R. Rubio, J. González-García, R. Costa, E. Pérez-Rodríguez, and A. Del Palacio, Impact of tuberculosis on the course of HIV-infected patients with a high initial CD4 lymphocyte count, *Int J Tuberc Lung Dis* **8** (2004), 451–7.

[54] L. A. Meyers, M. E. J. Newman, M. Martin, and S. Schrag, Applying network theory to epidemics: Control measures for Mycoplasma pneumoniae outbreaks, *Emerg. Infect. Dis.* **9** (2003), 204–210.
[55] D. Mollison, Dependence of epidemic and population velocities on basic parameters, *Math Biosci* **107** (1991), 255–287.
[56] R. S. Morris, D. U. Pfeiffer, and R. Jackson, The epidemiology of Mycobacterium-Bovis infections, *Veterinary Microbiology* **40** (1994), 153–177.
[57] C. J. L. Murray and J. A. Salomon, Modeling the impact of global tuberculosis control strategies, *Proceedings of the National Academy of Sciences of the United States of America* **95** (1998), 13881–13886.
[58] M. E. J. Newman, The structure and function of complex networks, *SIAM Rev.* **45** (2003), 167–256.
[59] L. M. O'Reilly and C. J. Daborn, The epidemiology of Mycobacterium bovis infection in animals and man: A review, *Tuber. Lung Dis.* **76** (1995), 1–46.
[60] A. Perelberg, D. Saltz, S. Bar-David, A. Dolev, and Y. Yom-Tov, Seasonal and circadian changes in the home ranges of reintroduced Persian fallow deer, *Journal of Wildlife Management* **67** (2003), 485–492.
[61] T. C. Porco, P. M. Small, and S. M. Blower, Amplification dynamics: Predicting the effect of HIV on tuberculosis outbreaks, *J. Acquir. Immune Defic. Syndr.* **28** (2001), 437–444.
[62] S. Riley, C. Fraser, C. A. Donnelly, A. C. Ghani, L. J. Abu-Raddad, A. J. Hedley, G. M. Leung, L.-M. Ho, T.-H. Lam, T. Q. Thach, P. Chau, K.-P. Chan, S.-V. Lo, P.-Y. Leung, T. Tsang, W. Ho, K.-H. Lee, E. M. C. Lau, N. M. Ferguson, and R. M. Anderson, Transmission dynamics of the etiological agent of SARS in Hong Kong: Impact of public health interventions, *Science* **300** (2003), 1961–1966.
[63] M. S. Sánchez, R. M. Grant, T. C. Porco, K. L. Gross, and W. M. Getz, Could a decrease in drug resistance levels of HIV be bad news?, *Bulletin Math. Biol.* (2005).
[64] L. Sattenspiel and C. P. Simon, The spread and persistence of infectious diseases in structured populations, *Mathematical Biosciences* **90** (1988), 341–366.
[65] M. T. Schechter, N. Le, K. J. P. Craib, T. N. Le, M. V. O'Shaughnessy, and J. S. G. Montaner, Use of the Markov model to estimate the waiting times in a modified WHO staging system for HIV infection, *Journal of Acquired Immune Deficiency Syndromes and Human Retrovirology* **8** (1995), 474–479.
[66] Z. Shen, F. Ning, W. G. Zhou, X. He, C. Y. Lin, D. P. Chin, Z. H. Zhu, and A. Schuchat, Superspreading SARS events, Beijing, 2003, *Emerg. Infect. Dis.* **10** (2004), 256–260.
[67] N. Shigesada and K. Kawasaki, *Biological Invasions: Theory and Practice*, Oxford University Press, New York, 1997.
[68] P. Sonnenberg, J. R. Glynn, K. Fielding, J. Murray, P. Godfrey-Faussett, and S. Shearer, How soon after infection with HIV does the risk of tuberculosis start to increase? A retrospective cohort study in South African gold miners, *J Infect Dis* **191** (2005), 150–158.
[69] M. Szykman, A. L. Engh, R. C. Van Horn, S. M. Funk, K. T. Scribner, and K. E. Holekamp, Association patterns among male and female spotted hyenas (Crocuta crocuta) reflect male mate choice, *Behavioral Ecology And Sociobiology* **50** (2001), 231–238.
[70] H. M. Taylor and S. Karlin, *An Introduction to Stochastic Modeling*, third ed., Academic Press, San Diego, 1998.
[71] C. P. B. Van der Ploeg, C. Van Vliet, S. J. De Vlas, J. O. Ndinya-Achola, L. Fransen, G. J. Van Oortmarssen, and J. D. F. Habbema, STDSIM: A microsimulation model for decision support in STD control, *Interfaces* **28** (1998), 84–100.
[72] J. Volmink, P. Matchaba, and P. Garner, Directly observed therapy and treatment adherence, *Lancet* **355** (2000), 1345–1350.
[73] J. Wallinga and P. Teunis, Different epidemic curves for severe acute respiratory syndrome reveal similar impacts of control measures, *Am. J. Epidemiol.* **160** (2004), 509–516.
[74] H. Wahlström, L. Englund, T. Carpenter, U. Emanuelson, A. Engvall, and I. Vagsholm, A Reed-Frost model of the spread of tuberculosis within seven Swedish extensive farmed fallow deer herds, *Preventive Veterinary Medicine* **35** (1998), 181–193.
[75] D. J. Watts and S. H. Strogatz, Collective dynamics of 'small-world' networks, *Nature* **393** (1998), 440–442.
[76] H. Whitehead, Testing association patterns of social animals, *Anim. Behav.* **57** (1999), 26–29.

[77] E. B. Wilson and J. Worcester, The spread of an epidemic, *Proceedings of the National Academy of Sciences* **31** (1945), 327–333.
[78] G. Wittemyer, I. Douglas-Hamilton, and W. M. Getz, The socio-ecology of elephants: analysis of the processes creating multi-tiered social structures, *Animal Behavior*, in press, 2005.
[79] M. E. J. Woolhouse, C. Dye, J. F. Etard, T. Smith, J. D. Charlwood, G. P. Garnett, P. Hagan, J. L. K. Hii, P. D. Ndhlovu, R. J. Quinnell, C. H. Watts, S. K. Chandiwana, and R. M. Anderson, Heterogeneities in the transmission of infectious agents: Implications for the design of control programs, *Proc. Natl. Acad. Sci. U. S. A.* **94** (1997), 338–342.
[80] Y. Xia, O. N. Bjornstad, B. T. Grenfell, Measles metapopulation dynamics: a gravity model for epidemiological coupling and dynamics, *Am. Nat.* **164** (2004), 267–281.

Department of Environmental Science, Policy and Management, 140 Mulford Hall #3112, University of California, Berkeley, CA 94720-3112, U.S.A., and Mammal Research Institute, Department of Zoology and Entomology, University of Pretoria, Pretoria 0002, South Africa

E-mail address: getz@nature.berkeley.edu

Biophysics Graduate Group, University of California at Berkeley

Department of Environmental Science, Policy and Management, 140 Mulford Hall #3112, University of California, Berkeley, CA 94720-3112, U.S.A., and Mammal Research Institute, Department of Zoology and Entomology, University of Pretoria, Pretoria 0002, South Africa

Department of Environmental Science, Policy and Management, 140 Mulford Hall #3112, University of California, Berkeley, CA 94720-3112, U.S.A.

Biophysics Graduate Group, University of California at Berkeley

California Department of Public Health

Department of Environmental Science, Policy and Management, 140 Mulford Hall #3112, University of California, Berkeley, CA 94720-3112, U.S.A.